1 FRONT MATTER

2 **Title**

- Full title: Climbing the crustal ladder: Magma storage-depth evolution during a volcanic flare-up
- *Short title:* Climbing the crustal ladder

5 Authors

- 6 Guilherme A. R. Gualda^{1*}, Darren M. Gravley², Michelle Connor¹, Brooke Hollmann¹, Ayla S. Pamukcu^{3,4},
- 7 Florence Bégué⁵, Mark S. Ghiorso⁶, Chad D. Deering⁷

8 Affiliations

- ¹ Vanderbilt University, Earth & Environmental Sciences, PMB 351805, Nashville, TN 37235, USA,
- 10 g.qualda@vanderbilt.edu.
- ² University of Canterbury, Geological Sciences, Christchurch, New Zealand.
- ³ Brown University, Providence, RI, USA.
- ⁴ Princeton University, Princeton, NJ, USA.
- ⁵ University of Lausanne, Institute of Earth Sciences, Lausanne, Switzerland.
- 15 ⁶ OFM Research West, Seattle, WA, USA.
- ⁷ Michigan Technological University, Houghton, MI, USA.

Abstract

Very large (>50 km³) to super (>450 km³) eruptions reveal the Earth's capacity to produce and store enormous quantities (>1000 km³) of crystal-poor, eruptible magma in the shallow crust. We explore the interplay between crustal evolution and volcanism during a volcanic flare-up in the Taupo Volcanic Zone (TVZ, New Zealand) using a combination of quartz-feldspar-melt equilibration pressures and timescales of quartz crystallization. Over the course of the flare-up, crystallization depths became progressively shallower, showing the gradual conditioning of the crust. Yet, quartz crystallization times were invariably very short (<100 years), demonstrating that very large reservoirs of eruptible magma were transient crustal features. We conclude that the dynamic nature of the TVZ crust favored magma eruption over storage. Episodic tapping of eruptible magmas likely prevented a supereruption. Instead, multiple very large bodies of eruptible magma were assembled and erupted in decadal timescales.

Science Advances

MAIN TEXT

Introduction

Very large (>50 km³) to super (>450 km³) eruptions expel hundreds of cubic kilometers of magma onto
the Earth's surface in a matter of days to months (1), unambiguously revealing the capacity of the Earths
shallow crust to store large quantities of eruptible magma (2). These magma bodies are predominantly –
though not exclusively – crystal poor, as revealed by the generally low crystal contents (<25 wt. %) of
the rocks formed from their eruptions. Eruptions of these magnitude – VEI \geq 7 (3) – can be catastrophic
to humankind at the local scale, with significant global impact (1, 4). Yet, our understanding of the
architecture of these systems and the processes associated with them is still limited. What are the
mechanisms whereby the Earth produces and collects such giant bodies of magma in relatively small
areas and feed these eruptions? What are the timescales over which these bodies of magma evolve prior
to eruption?
The everyone paradiam for the evigin of the eliter weeks on the idea of correction of evertal page manages
The current paradigm for the origin of rhyolites rests on the idea of segregation of crystal-poor magma
from a crystal-rich reservoir, the so-called Mush Model (5-7). Yet, the details of the depths at which
extraction of the crystal-poor magma takes place, the geometry of the magma bodies that are thus
established, and the connections between extracted and cumulate materials are still poorly understood.
Recent work suggests that discrete bodies of crystal-poor, eruptible magma feed very large and
supereruptions (8-11). Further, recent work reveals that the evolution of these magma bodies spans
different timescales (see 12). The crystal-rich reservoir has a relatively extended lifespan, from tens to
hundreds of thousands of years (13-16), possibly in excess of 1 Ma (17) – as revealed, for instance, by
timescales of zircon crystallization. But the eruptible magma bodies – formed by extracted magma – that
immediately feed eruptions are much shorter lived, recording quartz crystallization over centuries to
millennia (18-20). This short timescale suggests that once very large magma bodies are established, they
are unstable features in the shallow crust (21) that are prone to erupting. Most studies to date of very

large crystal-poor silicic deposits have focused on individual eruptions. Here, we explore the evolution of
eruptible magma bodies and associated crustal maturation in a system where repeated very large
eruptions took place in quick succession.

The Taupo Volcanic Zone (TVZ, New Zealand) is the volcanic region on Earth with the largest number of recent very large silicic caldera-forming eruptions (*22*). Over the last 350 ka, more than 4,000 km³ of magma have erupted in the TVZ, predominantly during 8 very large eruptions (>50 km³ of ejected material in each) concentrated over only ~70 ka – a remarkable 'ignimbrite flare-up' (*23*). This high productivity of silicic volcanism is linked to an intimate interplay between magmatic, tectonic and volcanic processes (*24*), yet evidence for these interacting processes has thus far been elusive. In this work, we explore the spatial and temporal variables that led to the accumulation and eruption of these very large bodies of eruptible magma in rapid succession. In the process, we gather critical information on the processes that lead to the formation of very large magma bodies during this flare-up, on the timescales of magma crystallization, and on the evolution of the shallow crust as heat and magma are transferred relatively rapidly into it. Our data reveal the interplay between crustal evolution and volcanism, and also explain how magma distribution varied over this short (~70 ka) period within the central TVZ crust.

Over the span of ~10 ka (350-340 ka), during the first pulse of the TVZ flare-up (*23*), a series of very large to supersized eruptions led to the formation of the Whakamaru and Paeroa pyroclastic deposits (*25*) – more than 2,000 km³ of material deposited through much of the central North Island (Fig. 1). With the end of the Whakamaru and Paeroa eruptions, major changes to the TVZ crust took place (*23*, *26*). The second pulse of the flare-up was marked by a change in the character of the erupted magmas (*23*): Whakamaru and Paeroa (*23*) magmas were characteristically cooler, more hydrous (as revealed by the abundance of hornblende), and commonly saturated in both sanidine and plagioclase; in contrast, magmas from the post-Whakamaru pulses 2 and 3 of the flare-up (*23*) were hotter and dryer, with plagioclase as the sole feldspar present (*26*) (see Table S1). In pulse 2 (Matahina, Chimpanzee, Pokai

eruptions), rocks include rare hornblende and show transitional character (particularly Matahina), while in pulse 3 (Mamaku, Ohakuri, Kaingaroa eruptions) the hot-dry assemblage with orthopyroxene as the dominant mafic mineral is characteristic (*23*).

Here, we use a multi-faceted approach that capitalizes on matrix glass and mineral compositions to probe the depths and timescales of magma storage within the TVZ crust during flare-up volcanism. We focus on 6 eruptions: Whakamaru, Matahina, Chimpanzee, Pokai, Mamaku, and Ohakuri that span the age and compositional spectrum of the TVZ flare-up. Our approach includes: (1) rhyolite-MELTS geobarometry (27) to calculate the pressures at which crystallization took place in these eruptible magma bodies and reveal the vertical organization of magmas over time in the flare-up; (2) determination of trace-element compositions of matrix glass to assess the compositional affinity of the various magmas that erupted during the flare-up; (3) cathodoluminescence (CL) zoning and modeling of Ti diffusion in quartz to infer the timescales over which these segregated, crystal-poor bodies of eruptible magma resided in the shallow crust prior to eruption (18, 19); and (4) phase-equilibria modeling with rhyolite-MELTS (28) to investigate crystallization histories and constrain the proportion of the total crystallization history recorded by quartz crystallization (19). In combination, these data lead to a comprehensive characterization of magma distribution in the shallow crust and of the rates of crystallization during the TVZ flare-up, with implications for understanding the evolving architecture of magmatic systems.

Results

Magma crystallization depths can be calculated using the rhyolite-MELTS (*28*) geobarometer (*27, 29, 30*), by calculating the pressure at which an assemblage of quartz and feldspars last equilibrated with melt of composition equal to that of observed glass. We interpret these pressures as those at which crystal-poor, eruptible magma was stored and crystallized prior to eruption. Our results using the rhyolite-MELTS geobarometer reveal a systematic spatial progression over the course of the flare-up (see Fig. 2). Our data suggest that Whakamaru magmas were stored and crystallized at pressures of <125 MPa. These

relatively low pressures (~5 km depth assuming shallow crust of 2,700 kg/km³) are consistent with prior estimates (*31*) for Whakamaru, and they are typical of magma storage pressures in the central TVZ (*29*). Following a period of ~20 ka of relative quiescence, caldera-forming eruptions were fed from magma bodies stored at progressively lower pressures, particularly on the western side of the central TVZ. On the eastern side of the central TVZ, Matahina magmas were stored at pressures of 100-170 MPa; on the western side, Chimpanzee magmas were stored at higher pressures, primarily 180-270 MPa (1 data point at 140 MPa). The western side of the central TVZ was the locus of renewed volcanism: the Chimpanzee eruption was followed by the Pokai eruption, and then by the almost simultaneous Mamaku and Ohakuri eruptions (*32*). Storage depths decreased over time: Pokai records pressures between 150 and 190 MPa (and a second population of 4 data points with pressures of ~50 MPa); Mamaku records pressures of 50 to 160 MPa (1 data point yielding 225 MPa); and pressures for Ohakuri are in the 50-100 MPa range. The lower pressures for Ohakuri and Mamaku are similar to those observed for Whakamaru and also typical of TVZ magmas (*29*).

Glass trace-element compositions reveal trends that are consistent with the patterns observed in crystallization pressures (Fig. 3). Matahina and Chimpanzee glass is the least evolved (e.g., higher Sr, lower LREE), while Mamaku and Ohakuri are the most evolved; Pokai glass compositions are generally intermediate between these two groups. Whakamaru glass shows compositions that do not align along the same trends (Fig. 3); this is likely due to the presence of sanidine, and it is consistent with the different nature of Whakamaru magmas (*23, 26*). Regardless of the mechanism that leads to such differences, we see an array of compositions that parallels the change in storage pressures over time.

We use quartz diffusion geochronometry using Ti concentration gradients (as revealed by CL zoning) in quartz crystals to probe crystallization times and growth rates during storage of crystal-poor, eruptible magmas that fed these eruptions (Fig. 4) (12, 18, 19). The origin of CL zoning in quartz is contentious (see 12) – while a common interpretation is that Ti correlates with temperature variations (33, 34), it is

now clear that Ti zonation can also result from variations in pressure (35, 36) and growth rate (37, 38).
Nonetheless, regardless of the specific origin, the existence of different zones in quartz allows
determination of crystallization times (see 18). In high-silica rhyolite magmas like the ones studied here,
the quartz stability field is only reached after crystallization of a feldspar (39), such that quartz is likely to
be consumed during waxing stages of a longer-lived magmatic system. In this sense, quartz differs
substantially from zircon and feldspars, which show substantial inheritance (14, 40-42) and record the
more extended history of waxing and waning of the magmatic systems in which they crystallize (12, 18).
As a result, quartz records crystallization only after establishment of very large crystal-poor, eruptible
magma bodies (12, 18, 19) – the magmas that ultimately feed eruptions. Even if quartz were to be partly
inherited, the crystallization times we determine are overestimates of the timescales of the magma
bodies that feed eruptions (18, 19).

In contrast to crystallization pressures and glass trace-element compositions, which vary substantially and systematically over time – particularly on the western central TVZ, crystallization times and average quartz growth rates are similar for all units studied (Fig. 5). For all units, calculated maximum crystallization times have modes between 10 and 100 a. The longest calculated time is 273 a, but 84% of all the calculated times are within 100 a before eruption. These results are consistent with existing results for Whakamaru magmas (20, 43). Resulting growth rates are also all very similar, with 74% of the calculated growth rates between 10^{-12} and 10^{-13} m/s (\sim 100-10 nm/day), similar to existing estimates for other systems (19). At these growth rates, a 1 mm diameter crystal (typical maximum size in the studied rocks) would grow in \sim 300 a, placing a maximum bound on the crystallization times for the units studied here.

Given that quartz is not the first phase to crystallize in rhyolitic magmas (39), we complement the quartz geochronometry data with rhyolite-MELTS simulations. Our goal is to assess the amount of crystallization – and the total time associated with it – that occurred prior to guartz saturation (18, 19). We assume that

heat loss by a magma body is nearly constant over time, such that crystallization time is proportional to enthalpy change (see 18, 19), which can be calculated using rhyolite-MELTS. The observed crystal contents in pumice can be used to constrain the total enthalpy loss, and the fraction of time prior to quartz saturation is given by the fraction of enthalpy lost in that crystallization span (18, 19). We assume that these magmas behaved as closed systems, which is consistent with the low crystal contents (<10 % crystals) of the erupted pumice studied here (see 19). Our results demonstrate that in the studied high-silica rhyolites, quartz saturation takes place at low total crystal content values (Fig. 6). Comparison of results from rhyolite-MELTS with observed crystal contents in pumice suggests that quartz was present in the crystallizing assemblage from 100% to 10% of the total crystallization time. This suggests that, in the worst case scenario, quartz crystallization times represent 10% of the total crystallization time, which leads to the conclusion that total crystallization time was no more than a millennium for the systems studied here. For the most part, crystallization times are likely much shorter than a millennium, possibly as short as decades. Centennial to millennial timescales are typical of other systems (18-20), which makes the decadal timescales determined here particularly short.

Discussion

In combination, these data suggest both a dramatic change in magma storage following the Whakamaru and Paeroa eruptions and a time progression in storage levels during pulses 2 and 3 of the TVZ flare-up. The changes in crystallization pressure and glass compositions from Whakamaru and Paeroa to pulse 2 magmas (i.e. Chimpanzee and Matahina rocks) are consistent with the idea that the Whakamaru magma system shut down at the end of the Whakamaru and Paeroa eruptions, being replaced by a new magmatic system (26). Our data reveal that subsequent to the shutdown of the Whakamaru and Paeroa magmatic system, new magmas were emplaced, crystallized, and fed eruptions from deeper regions in the crust, forming the units of pulse 2. With time, storage conditions became shallower, until pressures more typical of the central TVZ were established at the time of the Ohakuri and Mamaku eruptions (pulse

3). Interestingly, the shallower Pokai population may demonstrate early establishment of shallow magma
bodies. This evolution in the storage depths of magmas (particularly on the western central TVZ, from
Chimpanzee to Ohakuri) suggests eruptions emanating from new magma bodies that assembled quickly
as heat transfer from the deep crust remained high following Whakamaru volcanism. The exact
mechanisms that lead to this evolution in storage depths are not entirely understood. On the one hand,
the shallowing progression may have resulted from external forcing, for instance due to changes in the
tectonic controls imposed by crustal extension (24, 44). However, they can also have been controlled
internally, in response to the gradual conditioning of the crust due to the repeated intrusion of magma
(45) and consequent heat transfer into it (44). In fact, most likely, both factors have played their part, in
which case what our data reveals is a ladder-like evolution of magma storage depths as a result of the
interplay between tectonics and magmatism over time. This interplay between geologic processes has
been hypothesized and modelled for the TVZ (24, 45), but we present tangible evidence for the first time

The crystallization timescales we derive from quartz diffusion geochronometry reveal the timescales over which storage and crystallization of crystal-poor, eruptible magma take place – in other words, once established, coherent bodies of crystal-poor magma reside in the shallow crust until they ultimately feed eruptions, and we probe the timeframe between establishment of these bodies of magma and eruption (12, 18, 19). Our results show extremely short storage times for these eruptible magmas in the TVZ crust, on predominantly decadal timescales. Even after correction for the crystallization interval in which quartz was absent, storage times are still at most within centuries. This shows that these bodies of eruptible magma were somewhat transient features of the TVZ crust (18, 19). Importantly, these timescales are much shorter than the intervals between successive eruptions, suggesting that the eruptible magma bodies that fed these eruptions never coexisted. The unimodal distribution of crystallization pressures for any given eruption suggests that these eruptions did not result from direct mobilization and eruption of magmas from a dispersed source region (11). Rather, crystal-poor magmas collected and remained stored – albeit briefly – in coherent bodies from which eruptions were sourced.

The evidence points to sill-like bodies that span a narrow depth range, but more work is needed to better constrain the geometry of these magma bodies. The collection and storage of magmas in relatively shallow, discrete bodies are consistent also with the subsidence invariably observed following eruption and caldera collapse in the central TVZ (46, 47). Yet, the depths and timescales over which the segregation, collection, and extraction (from a deeper crystal-rich reservoir) of magma responsible for the establishment of these eruptible magma bodies is poorly understood, due to the lack of appropriate geobarometers and geochronometers that provide information on this stage of evolution.

The short lifetimes of the flare-up magma bodies following the Whakamaru event seem to indicate that conditions were ripe for eruption; whether – or, perhaps better stated, regardless of the extent to which – eruptions were internally triggered or externally assisted (21, 48-50), the conclusion is that the central TVZ crust was rather unstable during flare-up volcanism, favoring magma eruption over prolonged storage. We speculate that this dynamic tectono-magmatic environment prevented the buildup of a post-Whakamaru supereruption-size magma body (or set of magma bodies) in the central TVZ, and it favored eruption of smaller batches of magma. Had conditions been more stable, greater volumes of magma could have accumulated and been stored in the crust, potentially leading to the establishment of a supereruption-size body of eruptible magma. In this supereruptive scenario, the volume of magma would likely have waxed and waned over time (18, 40), leading to a more complex mosaic of multiple coexisting magma bodies, of variable dimensions, located over a wider range of depths (11). There is growing evidence that eventual destabilization and eruption of such mosaics of magma bodies are characteristic of supereruptions (8, 10, 51), even if the relatively organized sequential tapping of these magma bodies may appear to indicate the presence of a single, large, zoned magma body.

In combination, our data suggest establishment of discrete bodies of eruptible magma located at specific depths in the shallow crust. These bodies are rather unstable features of the shallow crust and they are prone to eruption by their own evolution (21, 48). This is consistent with recent work (18, 19, 52, 53)

that demonstrates that supereruption-forming magma bodies are ephemeral, being stored for no more than centuries to a few millennia before eruption. In other words, magma storage and eruption can happen on historical timescales. What we argue here is that, under special circumstances, very large (>50 km³) bodies of eruptible magma can develop even faster, leading to storage and eruption over decadal – i.e., human lifetime – timescales. What emerges is a scenario in which the central TVZ was a rapidly evolving system after the Whakamaru and Paeroa eruptions, with rapid magma generation, storage, and eruption, under varying conditions, as a response to the continuous transfer of heat and mass to the shallow crust.

Finally, understanding the organization of magma bodies in the crust and the timescales over which they evolve can ultimately prove relevant for hazard assessment and mitigation. Rapid magma evolution as seen in the case of the TVZ flare-up is seen in places where magmatic activity was persistent for much longer periods of time – as revealed, for instance, in the form of recurrent volcanism (e.g. TVZ) or a much longer record of crystallization preserved in zircon from the same system (e.g. Long Valley, California (13); Whakamaru, TVZ (16)). Given the magnitude of the potential impact of a supereruption on society, we suggest that monitoring of potentially restless calderas must include the specific search for clues that reveal mobilization and storage of large quantities of magma on timeframes of multiple years to decades.

Materials and Methods

We studied a total of 51 pumice clasts from 6 deposits (from older to younger; see Fig. 1): Whakamaru, Matahina, Chimpanzee, Pokai, Mamaku, and Ohakuri. Pumice clasts were lightly crushed using a baseball bat; after sieving, each size fraction was winnowed in water to separate crystal-rich from glass-rich fractions (*54*). Glass-coated, preferably whole, quartz crystals were hand-picked from the crystal-rich fractions and mounted in epoxy; mounts were ground to expose crystal interiors and polished down to 1

μm grit for CL imaging (18). We also prepared epoxy mounts of pieces of vesiculated glass from the
glass-rich fractions for matrix glass analysis.

We used a Tescan VEGA3 scanning electron microscope (SEM) with an attached panchromatic Tescan CL detector for CL imaging and an Oxford X-max 50 mm2 energy dispersive spectrometry (EDS) system for major-element compositional analysis. We used a 15 kV beam with specimen currents on the order of 3 nA for both CL imaging and EDS analysis. For CL imaging, we used a dwell time of 1 ms/pixel. For EDS analysis we used live acquisition times of 25 s, so as to minimize Na loss but yield measurable (i.e. above quantification limit) of minor elements, particularly Ti and Mg, which appear in concentrations between 0.1 and 0.5 oxide wt. %. Quality of the resulting analysis was checked by analyzing glass synthesized in the laboratory using the USGS reference powder RGM-1 (*55*) – results by Pamukcu et al. (*30*) using the same instrument and conditions demonstrate that our EDS analyses compare very well with reference values for RGM-1.

We used x-ray microfluorescence (56) to obtain Ti maps on the selected quartz crystals to investigate the correlation between CL intensity and Ti concentration. The x-ray microprobe at GeoSoilEnviroCARS uses the insertion device beamline 13IDC at the Advanced Photon Source (Argonne National Lab). We followed the procedures described in (12). The resolution of the obtained Ti maps is $<5 \mu m$ per pixel.

We used a ThermoFisher iCAP Qc quadrupole ICPMS coupled with a Photon Machines Excite 193 nm excimer laser ablation system (LA-ICPMS) for trace element analysis of matrix glass. The laser was set to a fluence of ~6 J/cm², a repetition rate of 10 Hz, 50 µm diameter, with He as carrier gas. Total analysis time was 90 s, including 20 s of pre-ablation, 60 s of ablation, and a 10 s interval prior to the next analysis. We used NIST 612 (57) as a primary standard and NIST 614 (58) and RGM-1 as secondary standards. We analyzed primary and secondary standards every 20-30 unknown measurements. Data processing was performed with the program Glitter (59), using Si as an internal standard. At least 20

analyses of glass in each sample were obtained,	and results were averaged after excluding outliers
(primarily due to mineral inclusions) (60).	

Magma crystallization depths were calculated with the rhyolite-MELTS geobarometer (27, 28) using the measured major-element glass compositions, as the pressures at which quartz and plagioclase are in equilibrium with a melt of the analyzed composition (27). A total of 88 out of 144 compositions yielded crystallization pressures, consistent with previous applications of the rhyolite-MELTS geobarometer (10, 27, 29, 30).

Crystallization timescales and average quartz growth rates were calculated using CL zoning as a proxy for Ti zoning (18, 19, 61). We assume profiles were initially step functions and calculate diffusion times using a 1D diffusion model from best-fit curves to measured profiles (18, 19); the assumption of a step function assures that we calculate maximum times for a given temperature, given that initial profiles may have been smoother than assumed. We used a set of routines developed in-house to extract intensity profiles from CL images and fit the appropriate error function to the extracted profiles. In all cases, we assume a temperature of 775 °C, consistent with existing temperature estimates for Whakamaru magmas (31, 43), and appropriate for all flare-up magmas. We calculate diffusion coefficients for Ti in quartz following the experimental work of Cherniak et al. (62). Uncertainties in the diffusion coefficient derive from the uncertainty in the activation energy, which is <5% 1 sigma (62) but appears in the exponential term of the diffusion equation, and uncertainties in temperature, which we assume to be 25 °C 1 sigma so as to encompass a wide range of possible temperatures (725-825 °C at the 2-sigma level). Following Gualda et al. (18), resulting errors in the calculated times are on the order of 150%; this level of uncertainty is small compared to other sources of error. Average growth rates (G) are calculated as the ratio between the growth distance (L) measured in the CL images (i.e. the distance between the zone boundary used for time estimates and the nearest crystal edge) and the growth time (t) calculated from the CL profiles (i.e. G = L/t; see Fig. 5) (12, 18, 19).

269

270

271

272

273

274

275

276

277

278

279

280

281

282

283

284

285

286

287

288

289

290

291

Rhyolite-MELTS (28) simulations were performed using MELTS_Excel (63). For each studied unit, we calculated an average of high-silica rhyolite compositions from data presented by Gravley et al. (23) (Table S2). Isobaric crystallization simulations were performed from liquidus to near solidus (\sim 10 wt. % liquid left), at pressures calculated here for that unit, assuming water saturation and an f_{O2} of NNO. The goal of the simulations was to determine the extent of crystallization of each magma prior to saturation in quartz. The choice of f_{O2} is not particularly important for these SiO₂-rich, low FeO and MgO magmas (28, 64).

References and Notes

293

294

295

296

297

298

299

- J. B. Lowenstern, R. B. Smith, D. P. Hill, Monitoring super-volcanoes: geophysical and geochemical signals at Yellowstone and other large caldera systems. *Philosophical Transactions of the Royal Society a-Mathematical Physical and Engineering Sciences* 364, 2055-2072 (2006).
- C. F. Miller, D. A. Wark, Supervolcanoes and their explosive supereruptions. *Elements* 4, 11-15
 (2008).
- 306 3. C. G. Newhall, S. Self, The Volcanic Explosivity Index (VEI): An estimate of explosive magnitude for historical volcanism. *Journal of Geophysical Research-Oceans* **87**, 1231-1238 (1982).
- S. Self, The effects and consequences of very large explosive volcanic eruptions. *Philosophical Transactions of the Royal Society a-Mathematical Physical and Engineering Sciences* 364, 2073-2097
 (2006).
- 5. O. Bachmann, G. W. Bergantz, On the origin of crystal-poor rhyolites: Extracted from batholithic crystal mushes. *Journal of Petrology* **45**, 1565-1582 (2004).
- 313 6. O. Bachmann, G. W. Bergantz, Rhyolites and their source mushes across tectonic settings. *Journal of Petrology* **49**, 2277-2285 (2008).

- 7. O. Bachmann, G. W. Bergantz, The magma reservoirs that feed supereruptions. *Elements* **4**, 17-21 (2008).
- 317 8. G. F. Cooper, C. J. N. Wilson, M.-A. Millet, J. A. Baker, E. G. C. Smith, Systematic tapping of
- 318 independent magma chambers during the 1 Ma Kidnappers supereruption. *Earth and Planetary*
- 319 *Science Letters* **313**, (2012).
- 320 9. F. Begue et al., Extraction, Storage and Eruption of Multiple Isolated Magma Batches in the Paired
- Mamaku and Ohakuri Eruption, Taupo Volcanic Zone, New Zealand. *Journal of Petrology* **55**, 1653-
- 322 1684 (2014).
- 323 10. G. A. R. Gualda, M. S. Ghiorso, The Bishop Tuff giant magma body: an alternative to the Standard
- 324 Model. *Contributions to Mineralogy and Petrology* **166**, 755-775 (2013).
- 325 11. K. V. Cashman, G. Giordano, Calderas and magma reservoirs. *Journal of Volcanology and*
- 326 *Geothermal Research* **288**, 28-45 (2014).
- 327 12. G. A. R. Gualda, S. R. Sutton, The Year Leading to a Supereruption. *Plos One* **11**, (2016).
- 328 13. J. I. Simon, M. R. Reid, The pace of rhyolite differentiation and storage in an 'archetypical' silicic
- magma system, Long Valley, California. *Earth and Planetary Science Letters* **235**, 123-140 (2005).
- 330 14. B. L. A. Charlier et al., Magma generation at a large, hyperactive silicic volcano (Taupo, New
- Zealand) revealed by U-Th and U-Pb systematics in zircons. *Journal of Petrology* **46**, 3-32 (2005).
- 332 15. C. J. N. Wilson, B. L. A. Charlier, Rapid Rates of Magma Generation at Contemporaneous Magma
- 333 Systems, Taupo Volcano, New Zealand: Insights from U-Th Model-age Spectra in Zircons. *Journal of*
- 334 *Petrology* **50**, 875-907 (2009).

- 335 16. S. J. A. Brown, I. R. Fletcher, SHRIMP U-Pb dating of the preeruption growth history of zircons from
- the 340 ka Whakamaru Ignimbrite, New Zealand: Evidence for > 250 k.y. magma residence times.
- 337 *Geology* **27**, 1035-1038 (1999).
- 17. J. F. Kaiser, S. de Silva, A. K. Schmitt, R. Economos, M. Sunagua, Million-year melt-presence in
- 339 monotonous intermediate magma fora volcanic-plutonic assemblage in the Central Andes:
- Contrasting histories of crystal-rich and crystal-poor super-sized silicic magmas. *Earth and Planetary*
- 341 *Science Letters* **457**, 73-86 (2017).
- 342 18. G. A. R. Gualda *et al.*, Timescales of quartz crystallization and the longevity of the Bishop giant
- magma body. *Plos One* **7**, e37492 (2012).
- 19. A. S. Pamukcu, G. A. R. Gualda, F. Begue, D. M. Gravley, Melt inclusion shapes: Timekeepers of
- short-lived giant magma bodies. *Geology* **43**, 947-950 (2015).
- 20. N. E. Matthews, C. Huber, D. M. Pyle, V. C. Smith, Timescales of Magma Recharge and Reactivation
- of Large Silicic Systems from Ti Diffusion in Quartz. *Journal of Petrology* **53**, 1385-1416 (2012).
- 348 21. L. Caricchi, C. Annen, J. Blundy, G. Simpson, V. Pinel, Frequency and magnitude of volcanic
- eruptions controlled by magma injection and buoyancy. *Nature Geoscience* **7**, 126-130 (2014).
- 350 22. C. J. N. Wilson et al., Volcanic and structural evolution of Taupo Volcanic Zone, New Zealand: A
- review. *Journal of Volcanology and Geothermal Research* **68**, 1-28 (1995).
- 352 23. D. M. Gravley, C. D. Deering, G. S. Leonard, J. V. Rowland, Ignimbrite flare-ups and their drivers: A
- 353 New Zealand perspective. *Earth-Science Reviews* **162**, 65-82 (2016).

- 354 24. C. Wilson, D. Gravley, G. Leonard, J. Rowland, Volcanism in the central Taupo Volcanic Zone, New
- 355 Zealand: tempo, styles, and controls. Studies in Volcanology: The Legacy of George Walker.
- 356 Special Publications of IAVCEI **2**, 225-247 (2009).
- 357 25. S. J. A. Brown, C. J. N. Wilson, J. W. Cole, J. Wooden, The Whakamaru group ignimbrites, Taupo
- 358 Volcanic Zone, New Zealand: evidence for reverse tapping of a zoned silicic magmatic system.
- *Journal of Volcanology and Geothermal Research* **84**, 1-37 (1998).
- 360 26. C. D. Deering, D. M. Gravley, T. A. Vogel, J. W. Cole, G. S. Leonard, Origins of cold-wet-oxidizing to
- 361 hot-dry-reducing rhyolite magma cycles and distribution in the Taupo Volcanic Zone, New Zealand.
- 362 Contributions to Mineralogy and Petrology **160**, 609-629 (2010).
- 363 27. G. A. R. Gualda, M. S. Ghiorso, Phase-equilibrium geobarometers for silicic rocks based on rhyolite-
- 364 MELTS. Part 1: Principles, procedures, and evaluation of the method. *Contributions to Mineralogy*
- 365 *and Petrology* **168**, (2014).
- 366 28. G. A. R. Gualda, M. S. Ghiorso, R. V. Lemons, T. L. Carley, Rhyolite-MELTS: A modified calibration of
- 367 MELTS optimized for silica-rich, fluid-bearing magmatic systems. *Journal of Petrology* **53**, 875-890
- 368 (2012).
- 369 29. F. Begue et al., Phase-equilibrium geobarometers for silicic rocks based on rhyolite-MELTS. Part 2:
- application to Taupo Volcanic Zone rhyolites. *Contributions to Mineralogy and Petrology* **168**,
- 371 (2014).
- 30. A. S. Pamukcu, G. A. R. Gualda, M. S. Ghiorso, C. F. Miller, R. G. McCracken, Phase-equilibrium
- geobarometers for silicic rocks based on rhyolite-MELTS-Part 3: Application to the Peach Spring Tuff
- 374 (Arizona-California-Nevada, USA). *Contributions To Mineralogy and Petrology* **169**, (2015).

- 37. N. E. Matthews et al., Quartz zoning and the pre-eruptive evolution of the similar to 340-ka
- Whakamaru magma systems, New Zealand. *Contributions to Mineralogy and Petrology* **163**, 87-107
- 377 (2012).
- 378 32. D. M. Gravley, C. J. N. Wilson, G. S. Leonard, J. W. Cole, Double trouble: Paired ignimbrite eruptions
- and collateral subsidence in the Taupo Volcanic Zone, New Zealand. *Geological Society of America*
- 380 *Bulletin* **119**, 18-30 (2007).
- 33. D. A. Wark, E. B. Watson, TitaniQ: a titanium-in-quartz geothermometer. *Contributions to*
- 382 *Mineralogy and Petrology* **152**, 743-754 (2006).
- 383 34. D. A. Wark, W. Hildreth, F. S. Spear, D. J. Cherniak, E. B. Watson, Pre-eruption recharge of the
- 384 Bishop magma system. *Geology* **35**, 235-238 (2007).
- 35. J. B. Thomas et al., TitaniQ under pressure: the effect of pressure and temperature on the solubility
- of Ti in quartz. *Contributions to Mineralogy and Petrology* **160**, 743-759 (2010).
- 38. J. B. Thomas, E. B. Watson, F. S. Spear, D. A. Wark, TitaniQ recrystallized: experimental
- confirmation of the original Ti-in-quartz calibrations. *Contributions to Mineralogy and Petrology* **169**,
- 389 16 (2015).
- 39. 37. R. Huang, A. Audetat, The titanium-in-quartz (TitaniQ) thermobarometer: A critical examination and
- re-calibration. *Geochimica Et Cosmochimica Acta* **84**, 75-89 (2012).
- 38. A. S. Pamukcu, M. S. Ghiorso, G. A. R. Gualda, The effect of growth rate on the production of Ti-
- and enriched rims of quartz phenocrysts in the Bishop magma bodies. 2015 AGU Fall Meeting
- 394 https://agu.confex.com/agu/fm15/meetingapp.cgi/Paper/64779, (2015).

- 39. G. A. R. Gualda, M. S. Ghiorso, Low-Pressure Origin of High-Silica Rhyolites and Granites. *Journal of Geology* **121**, 537-545 (2013).
- 397 40. K. M. Cooper, A. J. R. Kent, Rapid remobilization of magmatic crystals kept in cold storage. *Nature* 398 **506**, 480-+ (2014).
- 41. B. L. A. Charlier, C. J. N. Wilson, J. P. Davidson, Rapid open-system assembly of a large silicic magma body: time-resolved evidence from cored plagioclase crystals in the Oruanui eruption deposits, New Zealand. *Contributions to Mineralogy and Petrology* **156**, 799-813 (2008).
- 42. I. N. Bindeman, B. Fu, N. T. Kita, J. W. Valley, Origin and evolution of silicic magmatism at
 Yellowstone based on ion microprobe analysis of isotopically zoned zircons. *Journal of Petrology* 49,
 163-193 (2008).
- 43. K. E. Saunders, D. J. Morgan, J. A. Baker, R. J. Wysoczanski, The Magmatic Evolution of the
 406 Whakamaru Supereruption, New Zealand, Constrained by a Microanalytical Study of Plagioclase and
 407 Quartz. *Journal of Petrology* 51, 2465-2488 (2010).
- 40. C. D. Deering, O. Bachmann, J. Dufek, D. M. Gravley, Rift-Related Transition from Andesite to
 40. Rhyolite Volcanism in the Taupo Volcanic Zone (New Zealand) Controlled by Crystal-melt Dynamics
 41. in Mush Zones with Variable Mineral Assemblages. *Journal of Petrology* 52, 2243-2263 (2011).
- 45. J. V. Rowland, C. J. N. Wilson, D. M. Gravley, Spatial and temporal variations in magma-assisted
 rifting, Taupo Volcanic Zone, New Zealand. *Journal of Volcanology and Geothermal Research* 190,
 89-108 (2010).
- 414 46. C. J. N. Wilson *et al.*, Caldera volcanos of the Taupo Volcanic Zone, New Zealand. *Journal of Geophysical Research* **89**, 8463-8484 (1984).

- 416 47. J. W. Cole, D. M. Milner, K. D. Spinks, Calderas and caldera structures: a review. *Earth-Science*
- 417 *Reviews* **69**, 1-26 (2005).
- 418 48. S. Tramontano, G. A. R. Gualda, M. S. Ghiorso, Internal triggering of volcanic eruptions: Tracking
- overpressure regimes for giant magma bodies. *Earth and Planetary Science Letters* **472**, 142-151
- 420 (2017).
- 421 49. P. M. Gregg, S. L. de Silva, E. B. Grosfils, J. P. Parmigiani, Catastrophic caldera-forming eruptions:
- Thermomechanics and implications for eruption triggering and maximum caldera dimensions on
- 423 Earth. Journal of Volcanology and Geothermal Research **241**, 1-12 (2012).
- 424 50. P. M. Gregg, E. B. Grosfils, S. L. de Silva, Catastrophic caldera-forming eruptions II: The subordinate
- 425 role of magma buoyancy as an eruption trigger. *Journal of Volcanology and Geothermal Research*
- **305**, 100-113 (2015).
- 427 51. F. Béqué et al., Extraction, Storage and Eruption of Multiple Isolated Magma Batches in the Paired
- 428 Mamaku and Ohakuri Eruption, Taupo Volcanic Zone, New Zealand. *Journal of Petrology* **55**, 1653-
- 429 1684 (2014).
- 430 52. S. Seitz et al., Short magmatic residence times of quartz phenocrysts in Patagonian rhyolites
- associated with Gondwana breakup. *Geology* **44**, 67-70 (2016).
- 432 53. T. H. Druitt, F. Costa, E. Deloule, M. Dungan, B. Scaillet, Decadal to monthly timescales of magma
- transfer and reservoir growth at a caldera volcano. *Nature* **482**, 77-U97 (2012).
- 434 54. G. A. R. Gualda *et al.*, Fragmentation, nucleation and migration of crystals and bubbles in the Bishop
- Tuff rhyolitic magma. *Transactions of the Royal Society of Edinburgh-Earth Sciences* **95**, 375-390
- 436 (2004).

- 437 55. E. S. Gladney, I. Roelandts, 1987 compilation of elemental concentration data for USGS BHVO-1,
- 438 MAG-1, QLO-1, RGM-1, SCo-1, SDC-1, SGR-1, and STM-1. Geostandards Newsletter **12**, 253-362
- 439 (1988).
- 440 56. S. R. Sutton et al., Microfluorescence and microtomography analyses of heterogeneous Earth and
- 441 environmental materials. *Reviews in Mineralogy & Geochemistry* **49**, 429-483 (2002).
- 442 57. K. P. Jochum *et al.*, Determination of Reference Values for NIST SRM 610-617 Glasses Following ISO
- 443 Guidelines. *Geostandards and Geoanalytical Research* **35**, 397-429 (2011).
- 444 58. M. Kurosawa, S. E. Jackson, S. Sueno, Trace element analysis of NIST SRM 614 and 616 glass
- reference materials by laser ablation microprobe-inductively coupled plasma-mass spectrometry.
- 446 Geostandards Newsletter-the Journal of Geostandards and Geoanalysis 26, 75-84 (2002).
- 447 59. W. L. Griffin, W. J. Powell, N. J. Pearson, S. Y. O'Reilly, in *Laser Ablation-ICP-MS in the*
- 448 *Earth Sciences*. (2008), vol. 40, pp. 204-207.
- 449 60. A. J. Padilla, G. A. R. Gualda, Crystal-melt elemental partitioning in silicic magmatic systems: An
- 450 example from the Peach Spring Tuff high-silica rhyolite, Southwest USA. *Chemical Geology* **440**,
- 451 326-344 (2016).
- 452 61. W. P. Leeman et al., A Study of Cathodoluminescence and Trace Element Compositional Zoning in
- 453 Natural Quartz from Volcanic Rocks: Mapping Titanium Content in Quartz. *Microscopy and*
- 454 *Microanalysis* **18**, 1322-1341 (2012).
- 455 62. D. J. Cherniak, E. B. Watson, D. A. Wark, Ti diffusion in quartz. *Chemical Geology* **236**, 65-74
- 456 (2007).

457	63. G. A. R. Gualda, M. S. Ghiorso, MELTS_Excel: A Microsoft Excel-based MELTS interface for research						
458	and teaching of magma properties and evolution. Geochemistry Geophysics Geosystems 16, 315-						
459	324 (2015).						
460	CA M.C. Chiavas, C. A. D. Cualda, A mathed for actimating the activity of titania in magnetic liquids						
460	64. M. S. Ghiorso, G. A. R. Gualda, A method for estimating the activity of titania in magmatic liquids						
461	from the compositions of coexisting rhombohedral and cubic iron-titanium oxides. <i>Contributions To</i>						
462	Mineralogy and Petrology 165, 73-81 (2013).						
463	Acknowledgments						
464	General: We thank members of the MESSY group at Vanderbilt University for suggestions on the						
465	manuscript.						
466	Funding: This work was supported by the National Science Foundation (EAR-1151337) and by two						
467	Vanderbilt University Discovery Grants. Portions of this work were performed at GeoSoilEnviroCARS (The						
468	University of Chicago, Sector 13), Advanced Photon Source (APS), Argonne National Laboratory.						
469	GeoSoilEnviroCARS is supported by the National Science Foundation - Earth Sciences (EAR-1128799) and						
470	Department of Energy- GeoSciences (DE-FG02-94ER14466). This research used resources of the						
471	Advanced Photon Source, a U.S. Department of Energy (DOE) Office of Science User Facility operated for						
472	the DOE Office of Science by Argonne National Laboratory under Contract No. DE-AC02-06CH11357.						
473	Author contributions: GG and DG designed the study. GG, DG, MC, BH, AP, and FB conducted field						
474	work and sample collection. AP and FB contributed additional samples. MC and BH obtained the						
475	analytical data, with help and under the supervision of GG. MG performed thermodynamic calculations						
476	using rhyolite-MELTS, particularly pressure determinations. CD contributed knowledge on flare-up						
477	volcanism. GG and DG wrote the paper, and all authors revised it.						

Competing interests: No competing interests.

480 Figures and Tables

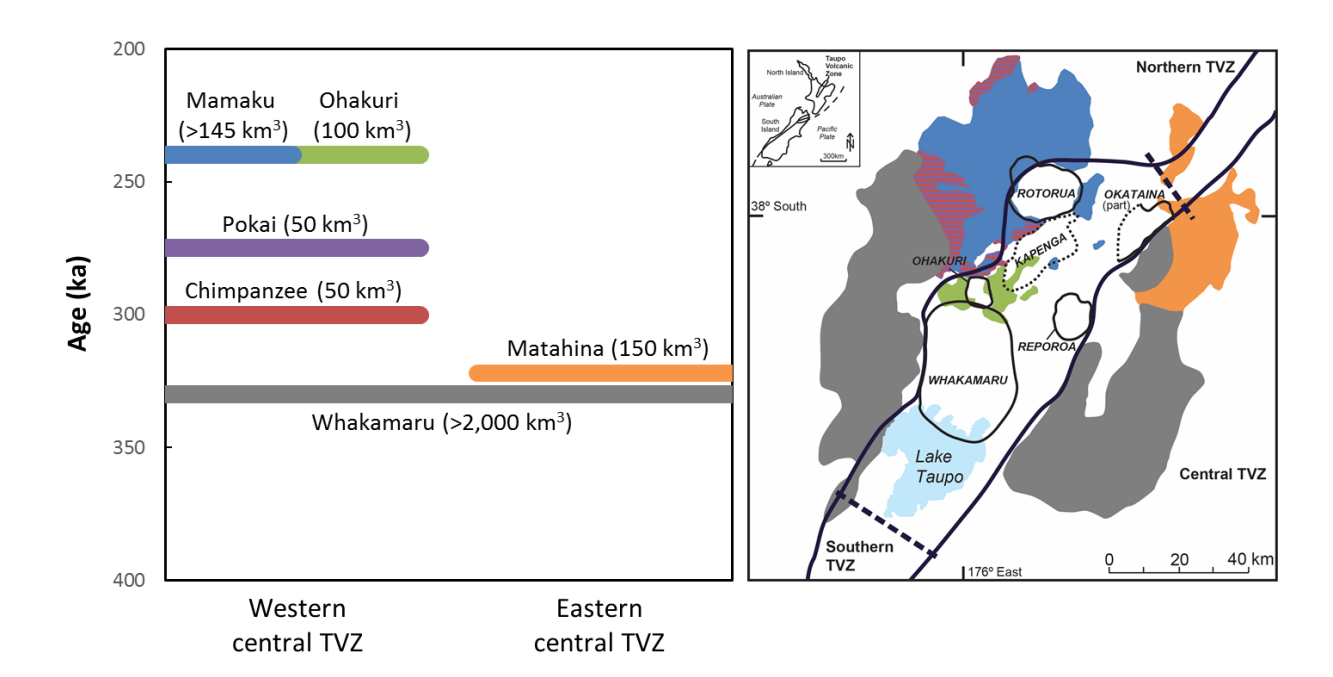


Fig. 1. Schematic showing the temporal evolution and map of the central Taupo Volcanic Zone (TVZ) highlighting the units of interest in this study. Key deposits are shown on both panels, with eruptive volumes indicated in parenthesis in left panel (see also Table S1). In left panel, vertical position of each bar represents best estimate for deposit age, while horizontal position of bars depicts whether deposits are part of the western or eastern central TVZ, or both. Color of units in map matches the colors on the diagram on the left.

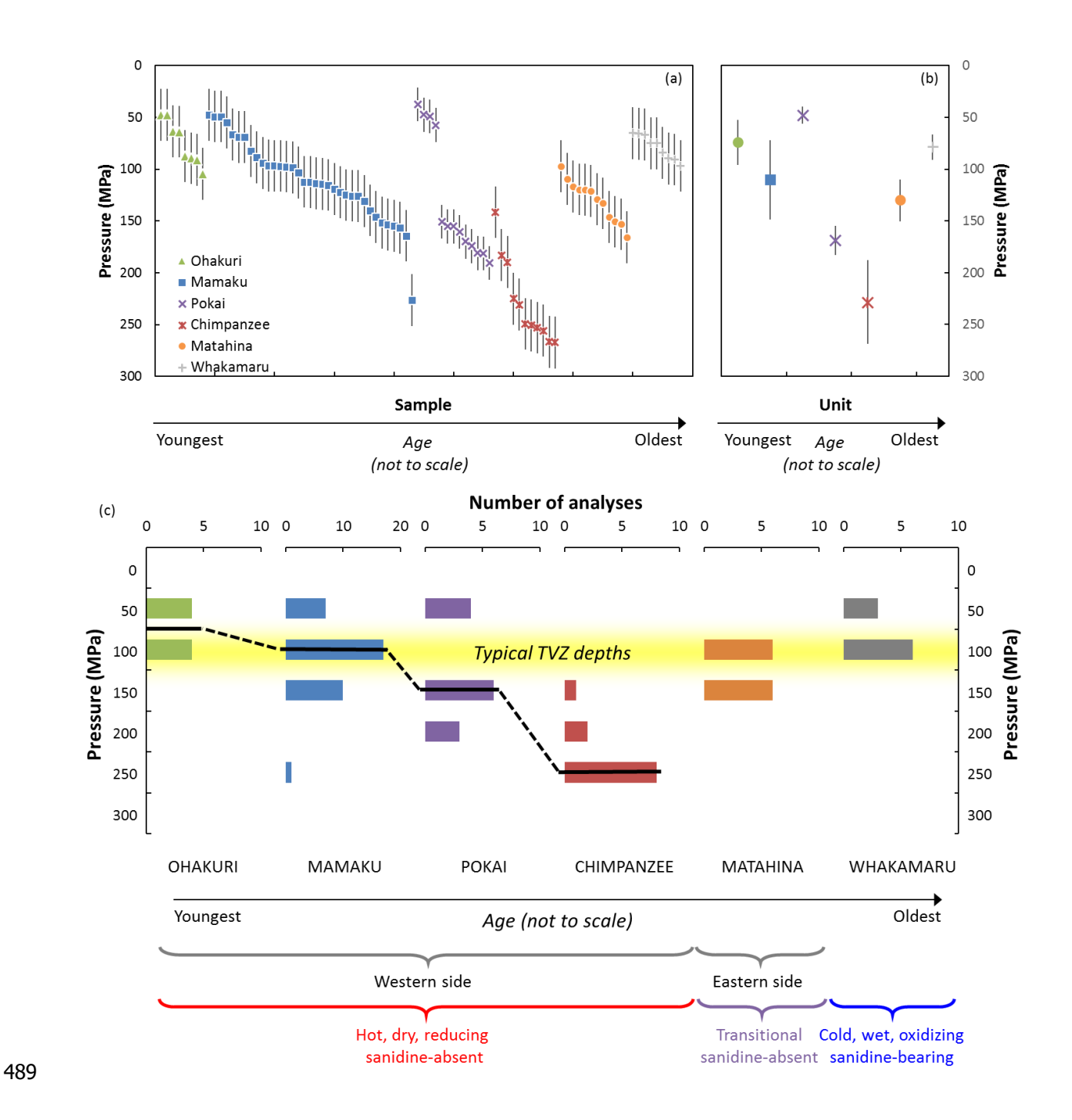


Fig. 2. **Crystallization pressures for magmas of the TVZ volcanic flare-up and late-Whakamaru Group.** (a) Each datapoint represents a single pressure determination based on rhyolite-MELTS calculations for a given matrix glass composition. Error bars are 25 MPa and represent our best estimate of the uncertainty associated with each determination(27). Different colors correspond to different

491

492

eruptive units. Eruptive units are organized according to age (increasing to the right), but individual samples are ordered according to crystallization pressure to facilitate visualization. (b) Each datapoint represents the average of all determinations for the corresponding unit (or subunit, in the case of Pokai); error bars are the standard deviation associated with that average. Units are organized according to age, like in (a); the ordering of Pokai subunits is arbitrary, with shallower subunit shown to the left for ease of visualization. (c) Bar diagrams of crystallization pressure for each unit. Diagrams are organized in order of increasing age, but age is not to scale. Vertical (pressure) axis is the same for all diagrams. Horizontal (number of analyses) scale is the same for all diagrams, except for Mamaku rocks, as indicated. Typical crystallization pressures for TVZ magmas derived from calculations by Bégué et al. (29) are indicated by yellow band. The data reveal a time progression for the storage depths of magmas feeding flare-up eruptions, particularly for the hot-dry-reducing magmas in the western portion of the central TVZ: storage starts at relatively deep levels for Chimpanzee magmas and gradually becomes shallower until the co-eruption of Mamaku and Ohakuri magmas.

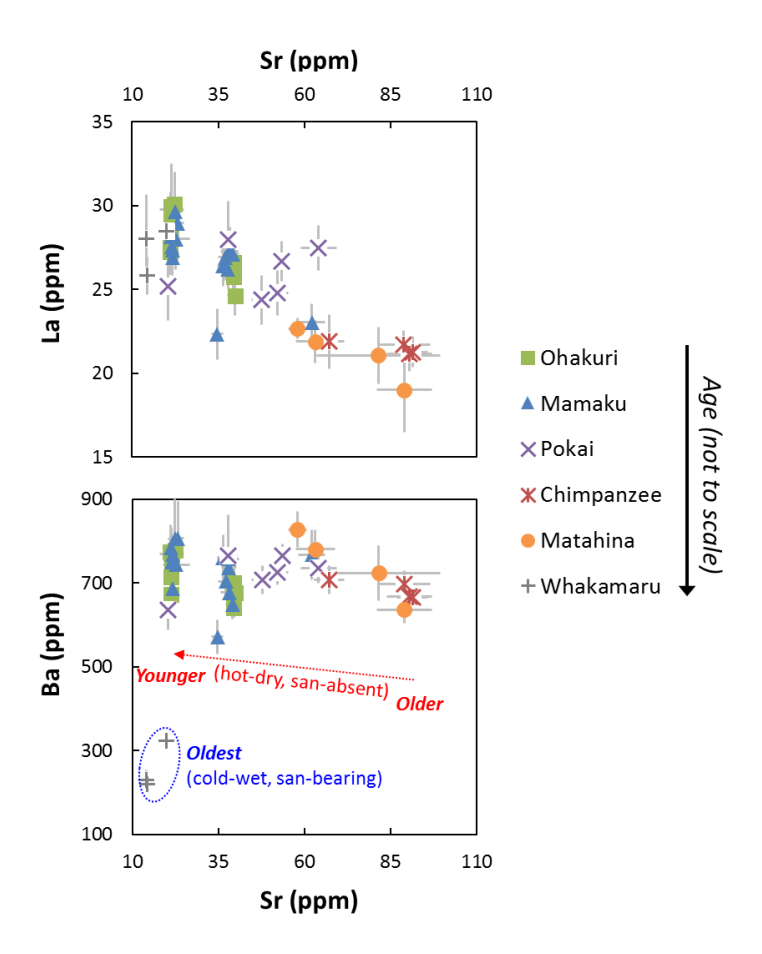
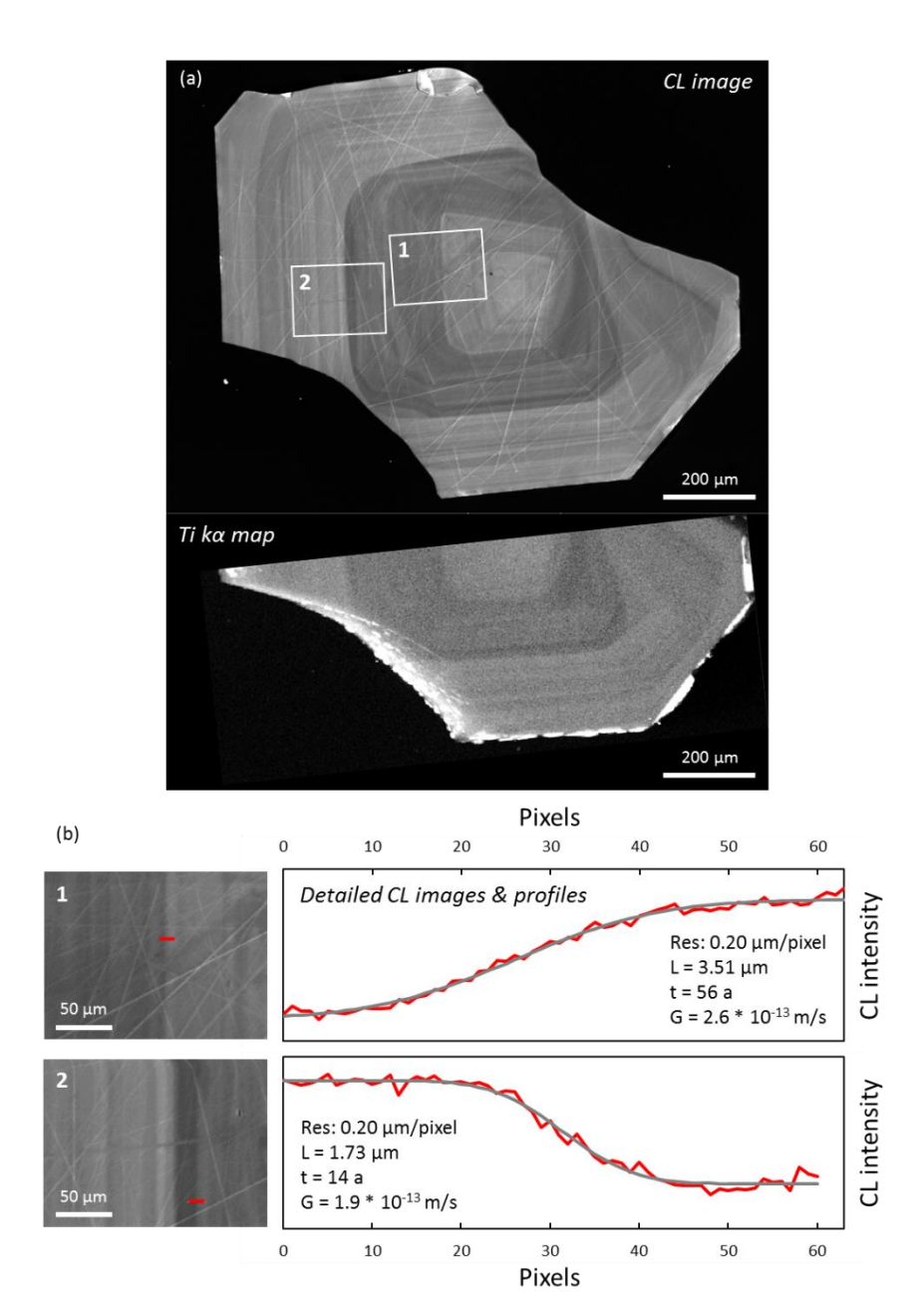


Fig. 3. Trace-element plots showing the compositional evolution of flare-up magmas in comparison with late-Whakamaru magmas. Whakamaru glass has very distinct Ba contents, probably a consequence of equilibration with sanidine. Flare-up magmas form a distinct array, with glass from older units (e.g. Chimpanzee) being less evolved (i.e., lower LREE, and higher Sr) than glass from younger units (e.g. Ohakuri), paralleling the time progression observed in crystallization pressures.



516 Fig. 4. Example of CL and Ti zoning in quarta

Fig. 4. Example of CL and Ti zoning in quartz, including calculation of growth time and rate from detailed CL images. CL image and Ti map shown in (a) demonstrate the correlation between CL intensity and Ti contents in quartz when there are large changes in CL; it can be seen that CL images capture the zoning in more detail, justifying the use of CL images for crystallization time and growth rate determination. Two areas were selected for detailed CL imaging, as indicated. (b) Detailed CL images

517

518

519

with corresponding profiles used for calculations of crystallization time and growth rate. Each observed
profile (red curve) is the average of 11 parallel profiles obtained from the image (shown in red in the
corresponding image). The best-fit error function is shown in gray, from which the characteristic diffusion
length (L) is extracted, which allows calculation of crystallization times (t). Calculation of growth rate (G)
requires obtaining the distance between the boundary and the edge of the crystal from the larger CL
image. See text for more details.

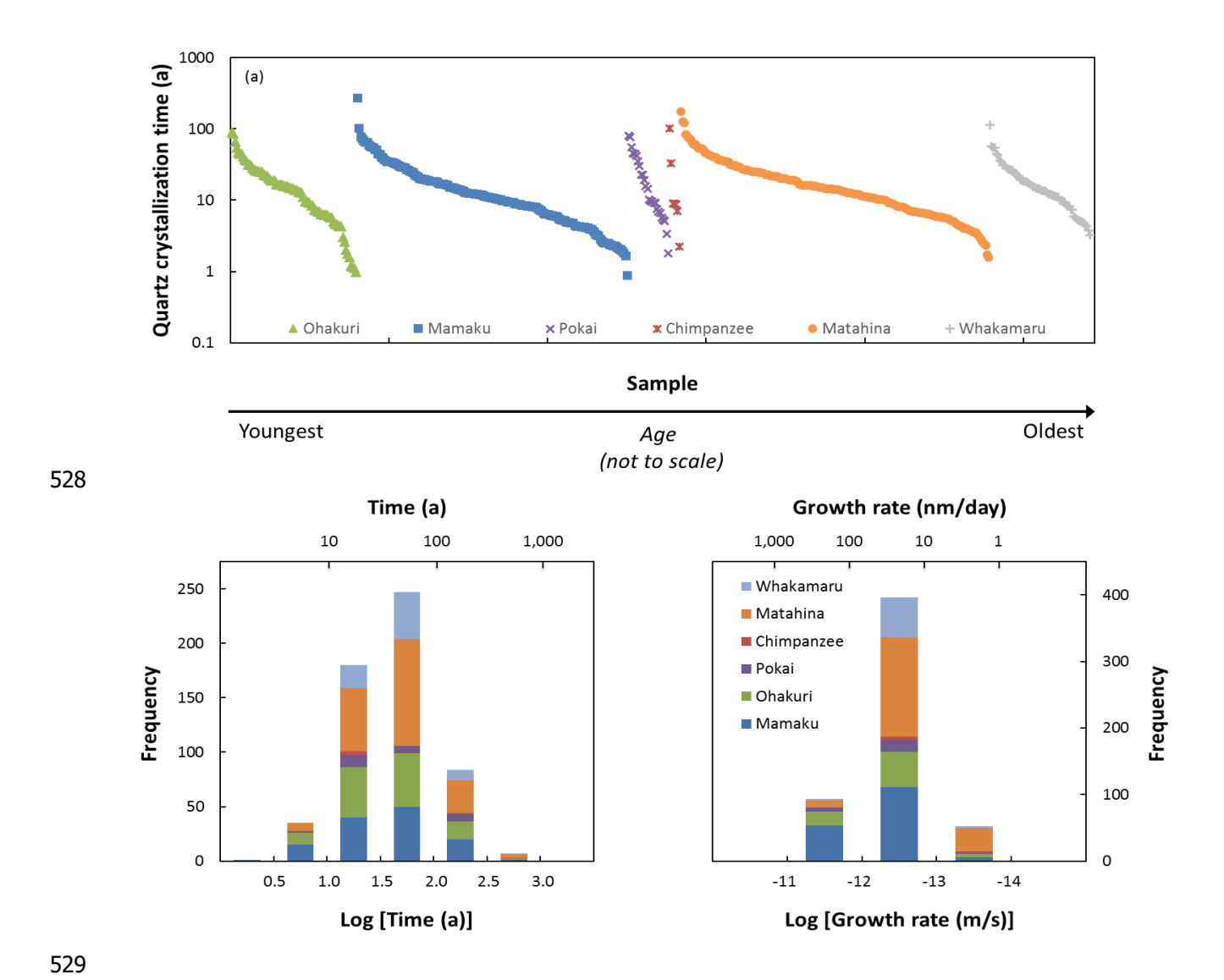


Fig. 5. Calculated crystallization times and growth rates for quartz from the TVZ volcanic flare-up and late-Whakamaru Group deposits. (a) Each datapoint represents an individual determination from a crystal from the corresponding unit. Units are organized according to age (increasing to the right), but individual datapoints for each unit are placed in order of increasing time to facilitate visualization. (b) Histogram showing distribution of crystallization times for each unit. (c) Histogram showing distribution of growth rates for each unit. The range of times is almost invariably within 1 and 100 years for all units, and growth rates are the same for all units.

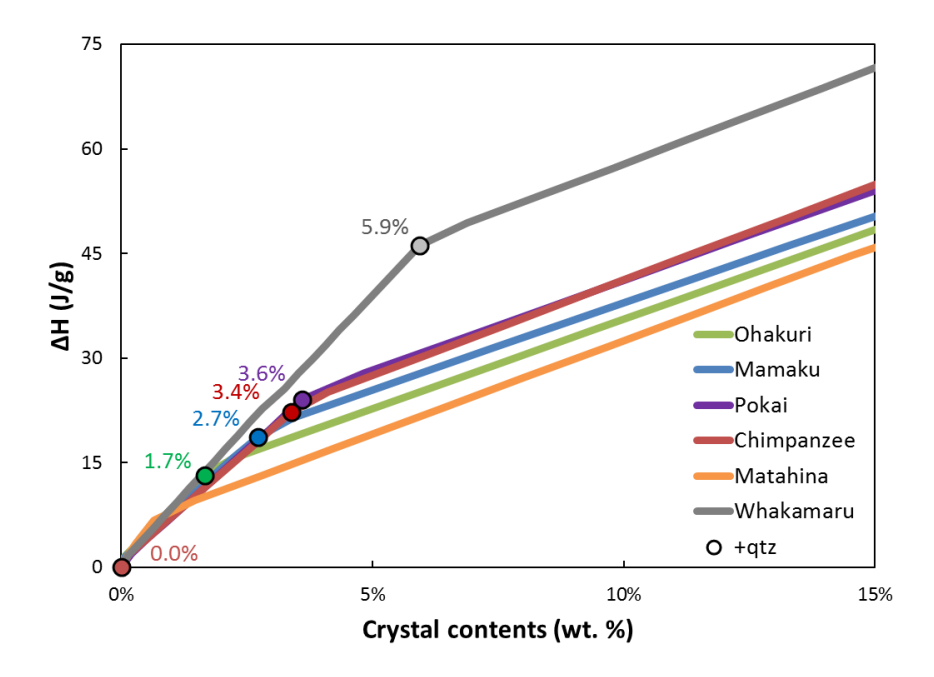


Fig. 6. Results of rhyolite-MELTS simulations showing the enthalpy lost over the course of crystallization for magmas from the TVZ volcanic flare-up and late-Whakamaru Group deposits. Each curve corresponds to the enthalpy loss from liquidus (crystal-free) conditions to 15 wt. % crystals. Plagioclase is a liquidus phase in all cases. The datapoints in each curve represent the crystal content and enthalpy at which the system saturates in quartz for that composition. Pressures used are the average for each unit (Fig. 2b). Water contents are set to yield fluid saturation at the liquidus, and f_{O2} is set to the Ni-NiO buffer. Starting compositions and pressure used are given in Table S2. Pumice from the TVZ flare-up typically contains <10 wt. % crystals, suggesting that measured quartz growth times (Fig. 5) in general correspond to at least 25% of the total crystallization times (under the limiting assumption that magmas were initially crystal free). For Whakamaru, crystal contents can be as high as 25 wt. % crystals. This suggests that crystallization times based on quartz crystallization times are typically within a factor of 4, and no more than within a factor of 10, of the total crystallization time.

Table S1. Characteristics of eruptive deposits from the central TVZ analyzed in this study.

Ignimbrite	Age (ka)	Volume (km³)	Source Caldera/ Caldera Complex	Crystal content (%)	Mineral assemblage (qtz + plg + opx)
Ohakuri	~240	~100	Ohakuri	< 10	
Mamaku	~240	> 145	Rotorua	< 10	± hbl
Pokai	~300	~50	Kapenga	< 15	
Chimpanzee	~320-300	~50	Kapenga	< 10	± hbl
Matahina	~320	~150	Okataina	< 15	± bt ± hbl
Whakamaru	~350	> 2,000	Whakamaru	< 35	+ san + bt + hbl

qtz-quartz; plg-plagioclase; opx-orthopyroxene; bt-biotite; hbl-hornblende; san-sanidine Modified from Gravley et al. (23).

552

553

Table S2. Magma compositions used for rhyolite-MELTS modeling of energy change associated with crystallization.

Composition*	Ohakuri	Mamaku	Pokai	Chimpanzee	Matahina	Whakamaru
SiO ₂	77.1	76.9	76.3	75.3	77.3	75.9
TiO ₂	0.15	0.15	0.15	0.20	0.12	0.16
Al_2O_3	12.8	13.1	13.3	13.9	13.1	13.8
FeO	1.32	1.27	1.48	1.73	1.17	1.34
MnO	0.06	0.04	0.06	0.07	0.04	0.04
MgO	0.13	0.10	0.11	0.15	0.20	0.13
CaO	0.82	0.73	0.85	1.14	0.86	1.06
Na₂O	3.53	3.96	3.82	3.86	3.45	3.16
K_2O	4.03	3.73	3.84	3.63	3.82	4.38
P_2O_5	0.02	0.02	0.03	0.03	0.01	0.02
Total	100.0	100.0	100.0	100.0	100.0	100.0
P (MPa) ^{\$}	74	111	132	228	130	79

^{*} Compositions determined from data in Gravley et al. (23)

^{\$} Pressures used are based on results from this study for the corresponding unit

Data file S1: Includes supplementary tables S3-S5.